

Subspace method based on neural networks for solving the partial differential equation in weak form

Pengyuan Liu^{a,c}, Zhaodong Xu^{a,c}, Zhiqiang Sheng^{a,b,*}

^a*National Key Laboratory of Computational Physics, Institute of Applied Physics and Computational Mathematics, Beijing, 100088, China*

^b*HEDPS, Center for Applied Physics and Technology, and College of Engineering, Peking University, Beijing, 100871, China*

^c*Graduate School of China Academy of Engineering Physics, Beijing 100088, China*

Abstract

We present a subspace method based on neural networks for solving the partial differential equation in weak form with high accuracy. The basic idea of our method is to use some functions based on neural networks as base functions to span a subspace, then find an approximate solution in this subspace. Training base functions and finding an approximate solution can be separated, that is different methods can be used to train these base functions, and different methods can also be used to find an approximate solution. In this paper, we find an approximate solution of the partial differential equation in the weak form. Our method can achieve high accuracy with low cost of training. Numerical examples show that the cost of training these base functions is low, and only one hundred to two thousand epochs are needed for most tests. The error of our method can fall below the level of 10^{-7} for some tests. The proposed method has the better performance in terms of the accuracy and computational cost.

Keywords: Subspace, neural networks, weak form, base function, training epochs.

*Corresponding author.

Email addresses: liupengyuan23@gscaep.ac.cn (Pengyuan Liu), xuzhaodong_math@163.com (Zhaodong Xu), sheng_zhiqiang@iapcm.ac.cn (Zhiqiang Sheng)

Preprint submitted to Elsevier

1. Introduction

Due to the rapid development of machine learning methods, the method based on neural networks attracts more and more attention. Many numerical methods based on neural networks have been proposed for solving the partial differential equation. Some of these methods are based on the strong form of the partial differential equation, such as physical information neural networks (PINN)[13], deep Galerkin method (DGM)[16], methods based on extreme learning machine (ELM)[3] and random feature methods (RFM) [1]. And others are based on the weak form of the partial differential equation, such as deep Ritz method (DRM)[4], and weak adversarial networks (WAN)[24].

The loss functions of PINN are based on the mean squared error consisting of information about the partial differential equation in strong form as well as the initial boundary conditions on some collocations points [5, 6, 9, 12, 22, 23]. The loss functions of DGM are based on the L^2 -norm of the residuals of partial differential equation in strong form. For these ELM-based methods and random feature methods, these parameters of neural networks are generated randomly and do not need to be updated, the approximate solution is given by solving a least-squares problem [2, 7, 10, 14, 17]. The loss function of the deep Ritz method is based on the energy functional corresponding to the weak form of partial differential equation. The weak adversarial networks method constructs a loss function by minimizing an operator norm induced from the weak form of partial differential equation.

The deep Ritz Method [4] uses the variational form of the partial differential equation as the loss function, and minimizes the loss function to update these parameters of neural networks. The deep Nitsche Method is proposed to deal with the essential boundary conditions in [8]. This method imposes the boundary conditions in a nonconforming way as the penalty method. A penalty-free neural network method for solving a class of second-order boundary-value problems on complex geometries is proposed in [15]. In which, the original problem is reformulated to a weak form so that the evaluations of high-order derivatives are avoided. An approach based on randomized neural networks and the Petrov-Galerkin method is developed in [14], in which finite element basis functions can be used as the test functions. A local randomized neural networks method with discontinuous Galerkin methods is proposed in [17], and the discontinuous Galerkin method is used to glue the solutions on sub-domains together. Some methods based on tensor neural networks for solving high-dimensional partial differential equation are

proposed in [18, 19, 20].

However, the accuracy of most methods is unsatisfactory, and the training cost is extremely high. It is a challenge to compete with traditional methods for low dimensional problems. A subspace method based on neural networks (SNN) for solving the partial differential equation in the strong form is proposed in [21]. The basic idea is to use some functions based on neural networks as base functions to span a subspace, then find an approximate solution in this subspace. Two special algorithms in the strong form of partial differential equation are designed. This method achieves high accuracy with low cost of training.

In this paper, we present a subspace method based on neural networks for solving the partial differential equation in the weak form (SNNW). First, we train these base functions in the subspace layer. These parameters of neural networks are updated by minimizing the loss function. The loss function can be based on different form, such as the strong form and the weak form. This means that these parameters can be updated by using various methods. We do not restrict the use of specific methods for training these base functions, and can use PINN, DGM or DRM to train these base functions in this step. After obtaining these base functions, we find an approximate solution of the partial differential equation in the weak form. Similar to [21], the loss function can include only the information of PDE and do not include the information of the initial boundary condition.

Numerical examples show that the cost of training these base functions is low, and only one hundred to two thousand epochs are needed for most tests. The error of our method can fall below the level of 10^{-7} for some tests. The performance of our method significantly surpasses the performance of existing methods based on the weak form of PDE in terms of the accuracy and computational cost.

The remainder of this paper is organized as follows. In section 2, we describe the subspace method based on neural networks for solving the partial differential equation in the weak form. In section 3, we present some numerical examples to test the performance of our method. At last, we give some conclusions.

2. SNN for solving the PDE in weak form

Consider the following equation:

$$\mathcal{A}u(\mathbf{x}) = f(\mathbf{x}) \quad \text{in } \Omega, \tag{1}$$

$$\mathcal{B}u(\mathbf{x}) = g(\mathbf{x}) \quad \text{on } \partial\Omega, \quad (2)$$

where $\mathbf{x} = (x_1, x_2, \dots, x_d)^T$, Ω is a bounded domain in \mathbb{R}^d , $\partial\Omega$ is the boundary of Ω , \mathcal{A} and \mathcal{B} are the differential operators, f and g are given functions.

2.1. Neural networks architecture

In this paper, we use the same neural networks architecture as [21]. For completeness, we briefly describe the neural networks architecture.

The neural networks architecture consists of four layers, which include input layer, hidden layers, subspace layer and output layer. Figure 1 illustrates the neural networks architecture.

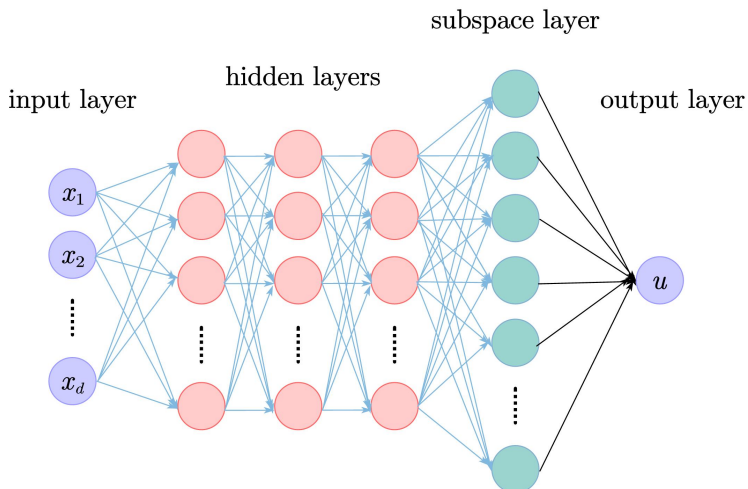


Figure 1: The neural networks architecture.

Let M be the dimension of subspace in the subspace layer, and $\varphi_j (j = 1, 2, \dots, M)$ be base functions of subspace, and $\omega_j (j = 1, 2, \dots, M)$ be some coefficients related to base functions. Denote $\varphi = (\varphi_1, \varphi_2, \dots, \varphi_M)^T$ and $\omega = (\omega_1, \omega_2, \dots, \omega_M)^T$. Let θ be the set of parameters in neural networks, $u(x; \theta, \omega)$ is the output with respect to input x with parameters θ and ω .

2.2. The training of base functions

We train the base functions of subspace such that the subspace has effective approximate capability to the solution space of equation.

In this step, we can use different methods to train the base functions of subspace. We describe how to train the base functions by using PINN, DGM and DRM.

2.2.1. The base functions based on PINN

To avoid introducing this penalty parameter, we define the following loss function which contains only the PDE loss term.

$$\mathcal{L}_D = \frac{1}{N} \sum_{j=1}^N (\mathcal{A}u(\mathbf{x}_j; \theta, \omega) - f(\mathbf{x}_j))^2. \quad (3)$$

It is obvious that this loss function includes only the information of PDE itself, and omit the information of initial boundary conditions.

First, we train the parameter θ and ω by minimizing the loss function $\mathcal{L}_D(\mathbf{x}; \theta, \omega)$ in (3). In order to balance the accuracy and efficiency, it is not necessary to solve the minimization problem accurately. Let $\mathcal{L}_{D_0}(\mathbf{x}; \theta, \omega)$ be the initial loss. The training process stops if the following condition is satisfied,

$$\frac{\mathcal{L}_D(\mathbf{x}; \theta, \omega)}{\mathcal{L}_{D_0}(\mathbf{x}; \theta, \omega)} \leq \varepsilon. \quad (4)$$

This implies that the training process stops if the loss decreases to a certain level. To prevent excessive training epochs, we introduce the maximum number of training epochs N_{max} . If the number of training epochs reaches N_{max} , the training process also stops.

2.2.2. The base functions based on DGM

Define the loss function as follows:

$$\mathcal{L}_I = \|\mathcal{A}u(\mathbf{x}; \theta, \omega) - f(\mathbf{x})\|_{L^2(\Omega)}^2. \quad (5)$$

We can see that the loss function includes only the information of PDE, and omit the information of initial boundary conditions.

At first, we train the parameter θ and ω by minimizing the loss function $\mathcal{L}_I(\mathbf{x}; \theta, \omega)$ in (5). Let $\mathcal{L}_{I_0}(\mathbf{x}; \theta, \omega)$ be the initial loss. The training process stops if the following condition is satisfied,

$$\frac{\mathcal{L}_I(\mathbf{x}; \theta, \omega)}{\mathcal{L}_{I_0}(\mathbf{x}; \theta, \omega)} \leq \varepsilon. \quad (6)$$

This implies that the training process stops if the loss decreases to a certain level. If the epochs reach N_{max} , the training process also stops.

2.2.3. The base functions based on DRM

Define the loss function as follows:

$$\mathcal{L}_R = \frac{1}{2}a(u(\mathbf{x}; \theta, \omega), u(\mathbf{x}; \theta, \omega)) - (f, u(\mathbf{x}; \theta, \omega)), \quad (7)$$

where $a(\cdot, \cdot)$ is a bilinear form that depends on the operators \mathcal{A} and \mathcal{B} . We will describe this bilinear form in the next subsection. Different from the loss function of PINN and DGM, the minimum value of the loss function \mathcal{L}_R is not 0. Hence, we can not use the relative loss to stop the training. In this paper, we can stop the training after the training epochs reach a given number.

2.3. The weak form

The equation (1) with the boundary condition (2) has the weak form: Find $u \in U$ such that

$$a(u, v) = (f, v), \quad \forall v \in V, \quad (8)$$

where U and V are two Hilbert spaces, $a(\cdot, \cdot)$ is a bilinear form that depends on the operators \mathcal{A} and \mathcal{B} .

We take the Poisson equation as the model problem to give the weak form. Consider the Poisson equation on the domain $\Omega = (0, 1) \times (0, 1)$,

$$-\Delta u = f, \quad \text{in } \Omega, \quad (9)$$

$$u = 0, \quad \text{on } \partial\Omega. \quad (10)$$

From (9), there is

$$-\int_{\Omega} \Delta u v dx = \int_{\Omega} f v dx, \quad \forall v \in H_0^1(\Omega). \quad (11)$$

By the Green's formula, we have

$$-\int_{\partial\Omega} \frac{\partial u}{\partial \mathbf{n}} v dx + \int_{\Omega} \nabla u \cdot \nabla v dx = \int_{\Omega} f v dx, \quad \forall v \in H_0^1(\Omega). \quad (12)$$

It follows

$$\int_{\Omega} \nabla u \cdot \nabla v dx = \int_{\Omega} f v dx, \quad \forall v \in H_0^1(\Omega). \quad (13)$$

Hence, we can get the following weak form:

$$a(u, v) = (f, v), \quad \forall v \in H_0^1(\Omega), \quad (14)$$

where

$$a(u, v) = \int_{\Omega} \nabla u \cdot \nabla v dx,$$

and

$$(f, v) = \int_{\Omega} f v dx.$$

In order to avoid the penalty on boundary condition, we simply use the following method to treat the Dirichlet boundary condition. For the problem (9)-(10), we multiply each $\bar{\varphi}_j$ by the limit function $h : x(1-x)y(1-y)$ to obtain the homogeneous trial function subspace as follows:

$$\varphi_j = x(1-x)y(1-y)\bar{\varphi}_j, \quad j = 1, \dots, M.$$

where φ_j and $\bar{\varphi}_j$ are obtained by the training process of subspace layer in section 2.2. It should be pointed out that there are many choices of the limiting function h as long as they satisfy the condition of being zero on $\partial\Omega$ and nonzero in Ω .

Define the finite dimensional space $V_h = \text{span}\{\varphi_1, \varphi_2, \dots, \varphi_M\}$. The corresponding weak form: Find $u_h \in V_h$ such that

$$a(u_h, v_h) = (f, v_h), \quad \forall v_h \in V_h. \quad (15)$$

Note that u_h can be expressed as

$$u_h = \sum_{j=1}^M \omega_j \varphi_j. \quad (16)$$

Inserting (16) into (15), and setting $v_h = \varphi_i, i = 1, \dots, M$, we obtain

$$\sum_{j=1}^M \omega_j a(\varphi_j, \varphi_i) = (f, \varphi_i), \quad i = 1, 2, \dots, M. \quad (17)$$

From (17), we can get a linear system

$$A\omega = b, \quad (18)$$

where A is a $M \times M$ matrix with $A_{ij} = a(\varphi_j, \varphi_i)$ and b is a $M \times 1$ vector with $b_i = (f, \varphi_i)$. Solve the linear system (18) to obtain ω , and then the approximate solution is obtained by (16).

We summarize the main steps of our method as follows:

Algorithm: SNNW

1. Initialize neural networks architecture.
 2. Generate randomly θ and ω .
 3. Update parameter θ and ω by minimizing the loss function $\mathcal{L}(\mathbf{x}; \theta, \omega)$ until stop criteria is satisfied.
 4. Obtain the base functions of the subspace $\varphi_1, \varphi_2, \dots, \varphi_M$.
 5. Solve the algebraic system (18) resulted from (15) in weak form to update ω .
 6. Obtain an approximate solution u_h .
-

Different loss function leads different method. SNNW based on the base functions in Section 2.2.1 is denoted as SNNW-P, SNNW based on the base functions in Section 2.2.2 is denoted as SNNW-G, and SNNW based on the base functions in Section 2.2.3 is denoted as SNNW-R.

3. Numerical results

In this section, we use some numerical experiments to test our method. In Section 3.1, we test the performance of SNNW by solving the one-dimensional Helmholtz equation. In Section 3.2, we test our method for solving the Poisson equation. In Section 3.3, we solve the diffusion equation with strongly anisotropic ratios.

We employ the framework PyTorch [11], and all variable data types are set to float64. We maintain consistent settings for all numerical tests in this paper. Specifically, we use a feedforward fully connected neural network with four hidden layers, each containing 100 neurons. The activation function is the Tanh function, the subspace dimension is 300, the optimizer is Adam and the settings of optimizer are kept at their default values. Neural network parameters are randomly generated by using the Xavier method. In order to accurately reproduce numerical results, the seed for generating random numbers in all numerical experiments is set to 1.

For SNNW-P and SNNW-G, the training process stops when the relative loss is less than ε or the epochs reach N_{max} . For SNNW-R, the training process stops when the epochs reach 2000. In all tests, we take $\varepsilon = 1e - 3$ and $N_{max} = 5000$.

We compare our method with the existing methods, including PINN, DGM and DRM. For comparison purposes, identical network architectures, parameter settings, and initialization methods are employed for PINN, DGM and DRM, with the Adam optimizer training through 50000 epochs.

We use the following relative L^2 error to evaluate the accuracy,

$$\|e\|_{L^2} = \frac{\sqrt{\sum_{i=1}^N |u_h(X_i) - u^*(X_i)|^2}}{\sqrt{\sum_{i=1}^N |u^*(X_i)|^2}},$$

where u^* is the exact solution.

3.1. Helmholtz equation

Consider the 1D Helmholtz equation with the Dirichlet boundary conditions as follows:

$$\begin{aligned} -u_{xx} + \lambda u &= f, \quad a < x < b, \\ u(a) &= 0, \quad u(b) = 0. \end{aligned}$$

The exact solution is taken as

$$u(x) = \sin(3\pi x) + \cos\left(4\pi x + \frac{1}{2}\pi\right),$$

where $a = 0$, $b = 2$, $\lambda = 1$.

To obtain the integration in weak form of SNNW directly, the complex Gaussian points are chosen in training process. The complex Gaussian quadrature formula is applied to segment $[a, b]$ into 100 sub-intervals, with each sub-interval containing 10 points.

Table 1 shows the relative L^2 error for different methods. Obviously, the errors of PINN, DGM and DRM are between 10^{-3} and 10^{-4} after 50000 training epochs. We can see that SNNW-P achieves relative L^2 error of 3.50e-06 with only 250 epochs, SNNW-G achieves relative L^2 error of 6.73e-06 with only 273 epochs, and SNNW-R achieves relative L^2 error of 5.65e-06 with 2000 epochs. This demonstrates that the performance of SNNW has the superiority in the accuracy and training cost.

The numerical solutions obtained by our SNNW method are shown in Figure 2. Figure 3 illustrates the point-wise errors of our methods.

The numerical results of SNNW-P and SNNW-G are displayed for various numbers of sampling points and subspace dimension in Tables 2 and 3. The

Table 1: The errors and epochs of different methods for the Helmholtz equation

Method	$\ e\ _{L^2}$	epochs
PINN	5.63e-03	50000
DGM	2.29e-04	50000
DRM	4.51e-03	50000
SNNW-P	3.50e-06	250
SNNW-G	6.73e-06	273
SNNW-R	5.65e-06	2000

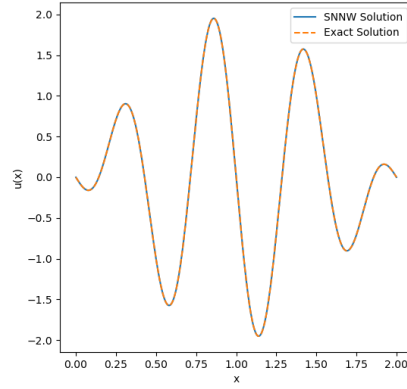


Figure 2: Solution obtained by SNNW for Helmholtz Equation.

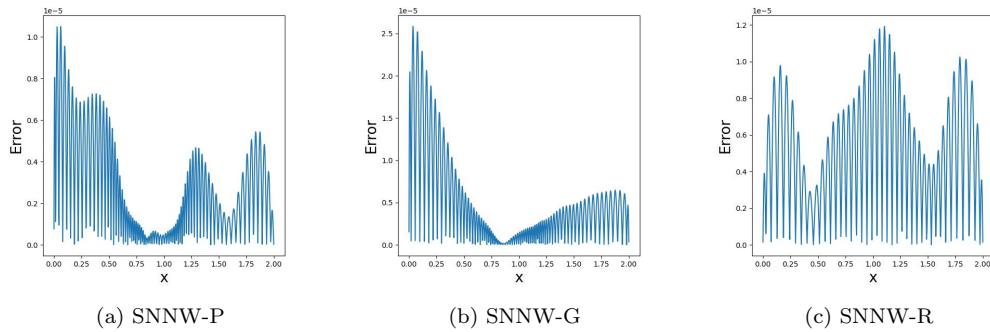


Figure 3: Point-wise errors of SNNW-P, SNNW-G and SNNW-R for Helmholtz equation.

network setup is uniform with four hidden layers, each with 100 neurons and adopts the composite Gaussian quadrature rule, sampling 10 points per sub-interval and incrementing sub-interval counts for accuracy enhancement. With the sampling point number of 60 and 80, the accuracy is not satisfied. This means that there needs more sampling points to obtain better accuracy. Increasing the number of sampling point to 200, SNNW-P and SNNW-G can achieve rapidly the accuracy of 10^{-5} . As the number of sampling points and subspace dimension increases, both SNNW-P and SNNW-G can obtain the stable accuracy of 10^{-6} . Moreover, the number of training epochs is between 200 and 3000.

Table 2: The errors and epochs of SNNW-P across various numbers of sampling points and subspace dimension M for the Helmholtz equation.

Points	M	60	80	100	300	500
60	$\ e\ _{L^2}$	4.33e01	1.12e02	6.66e01	5.04e01	9.98e00
	epochs	2329	399	1406	366	506
80	$\ e\ _{L^2}$	3.85e00	1.45e01	4.15e01	8.71e-01	3.77e-03
	epochs	994	721	1029	431	285
100	$\ e\ _{L^2}$	2.06e-03	4.69e-04	6.76e-03	8.85e00	2.79e-04
	epochs	347	287	307	288	298
200	$\ e\ _{L^2}$	9.56e-05	4.46e-06	1.33e-05	1.13e-05	1.75e-06
	epochs	275	261	574	309	280
300	$\ e\ _{L^2}$	9.40e-05	2.10e-05	2.78e-05	4.36e-06	1.09e-06
	epochs	352	321	660	298	258
500	$\ e\ _{L^2}$	1.37e-04	4.64e-05	3.01e-05	5.94e-06	1.60e-06
	epochs	267	430	807	276	249
1000	$\ e\ _{L^2}$	6.67e-05	7.94e-05	2.70e-05	3.40e-06	1.46e-06
	epochs	295	420	676	282	250

Similar to SNNW-P and SNNW-G, SNNW-R has the same network setup and composite Gaussian quadrature rule. The numerical results of SNNW-R with given 2000 epochs are shown in Table 4 for various numbers of sampling points and subspace dimension. The accuracy is not satisfied when the number of sampling point number is small. Increasing the number of sampling points and subspace dimension, SNNW-R obtains the accuracy of

Table 3: The errors and epochs of SNNW-G across various numbers of sampling points and subspace dimension M for the Helmholtz equation.

Points	M	60	80	100	300	500
60	$\ e\ _{L^2}$	7.85e01	6.25e01	6.31e01	4.94e01	9.43e-02
	epochs	537	330	2202	396	354
80	$\ e\ _{L^2}$	8.38e-01	2.52e01	4.66e01	1.91e01	3.13e-04
	epochs	449	378	1211	583	260
100	$\ e\ _{L^2}$	1.84e-03	5.10e-01	8.88e-04	7.42e-04	1.48e-03
	epochs	305	584	440	284	302
200	$\ e\ _{L^2}$	1.65e-04	7.67e-05	6.11e-05	2.38e-05	2.43e-06
	epochs	310	531	425	245	300
300	$\ e\ _{L^2}$	8.62e-05	7.04e-05	1.86e-05	2.58e-06	3.05e-06
	epochs	286	324	365	246	268
500	$\ e\ _{L^2}$	1.01e-04	3.11e-05	3.04e-05	6.30e-06	3.32e-06
	epochs	307	347	381	270	267
1000	$\ e\ _{L^2}$	1.23e-04	1.64e-05	1.92e-05	6.73e-06	3.19e-06
	epochs	314	316	362	273	248

10^{-5} . The number of training epochs of our methods is significantly less than that required by PINN, DGM and DRM.

Table 4: The errors of SNNW-R with 2000 epochs across various numbers of sampling points and subspace dimension M for the Helmholtz equation

Points	M	60	80	100	200	300	500
60	$\ e\ _{L^2}$	3.00e01	3.59e01	2.81e01	6.51e00	6.30e-04	7.38e-04
80	$\ e\ _{L^2}$	1.38e-03	1.13e-02	7.52e-02	9.39e-03	7.58e-06	1.05e-05
100	$\ e\ _{L^2}$	1.50e-04	1.42e-04	1.18e-03	3.79e-05	6.10e-06	1.30e-05
200	$\ e\ _{L^2}$	9.06e-05	5.06e-06	5.00e-06	2.39e-06	5.64e-06	1.27e-05
300	$\ e\ _{L^2}$	8.98e-05	6.38e-06	5.04e-06	2.09e-06	5.74e-06	1.24e-05
500	$\ e\ _{L^2}$	1.02e-04	6.65e-06	5.06e-06	2.16e-06	5.53e-06	1.26e-05
1000	$\ e\ _{L^2}$	1.00e-04	6.46e-06	5.07e-06	2.39e-06	5.65e-06	1.25e-05

Now we test the variation pattern of errors. First, the number of sampling points is given, we examine the error variation with respect to subspace dimension. Then, the subspace dimension is fixed, we examine the error variation with respect to the number of sampling points. Figure 4 illustrates the error variation with subspace dimension for 1000 sampling points, and the error variation with the number of sampling points for a fixed subspace dimension of 300 for SNNW-P. Similarly, Figure 5 and 6 show the variation pattern of errors for SNNW-G and SNNW-R, respectively.

Table 5 presents the results of SNNW-P for different hidden layer depth and subspace dimension, maintaining a uniform width of 100 for each hidden layer. When the number of the subspace dimension is 60, the accuracy is not satisfied. When the number of the subspace dimension is 300, the error of SNNW-P is between 10^{-5} and 10^{-7} , and the depth of hidden layer has no significant impact on accuracy. For SNNW-G and SNNW-R, there has similar results.

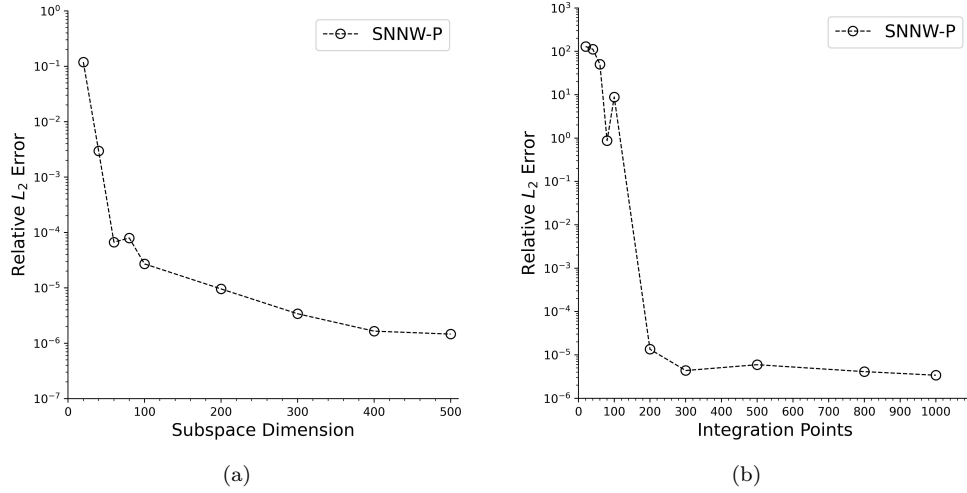


Figure 4: Error variation with subspace dimension at a fixed number of 1000 sampling points and error variation with the number of sampling points at a fixed subspace dimension of 300 for SNNW-P.

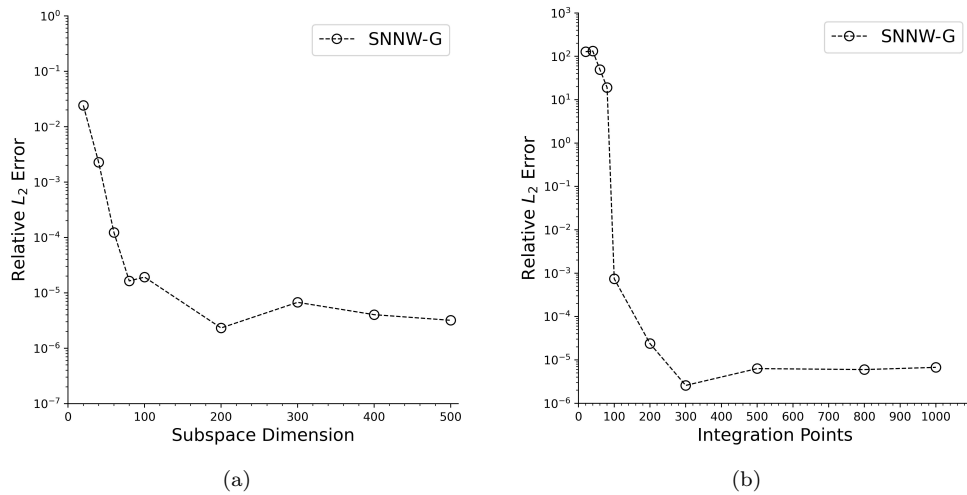


Figure 5: Error variation with subspace dimension at a fixed number of 1000 sampling points and error variation with the number of sampling points at a fixed subspace dimension of 300 for SNNW-G.

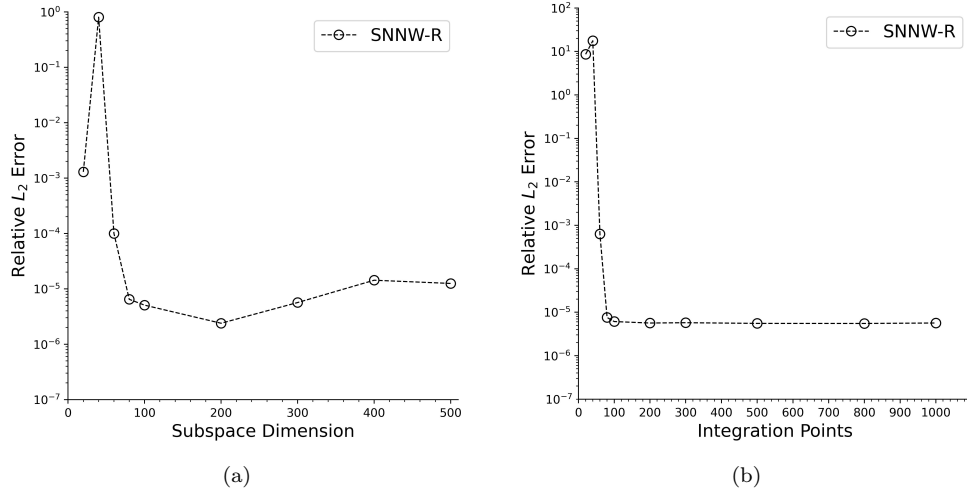


Figure 6: Error variation with subspace dimension at a fixed number of 1000 sampling points and error variation with the number of sampling points at a fixed subspace dimension of 300 for SNNW-R.

Table 5: The errors and epochs for SNNW-P on different hidden layer depth.

Hidden Layer	M	60	100	300
0	$\ e\ _{L^2}$	1.11e-05	1.27e-05	2.39e-06
	epochs	3340	2600	1902
1	$\ e\ _{L^2}$	2.01e-03	3.39e-04	3.33e-07
	epochs	2540	860	254
2	$\ e\ _{L^2}$	3.49e-01	8.29e-05	2.42e-05
	epochs	5000	1415	406
3	$\ e\ _{L^2}$	2.41e-04	1.42e-05	1.94e-06
	epochs	393	233	213
4	$\ e\ _{L^2}$	6.67e-05	2.714e-05	3.39e-06
	epochs	295	676	282
5	$\ e\ _{L^2}$	1.01e-03	1.32e-04	3.90e-06
	epochs	1465	456	275
6	$\ e\ _{L^2}$	5.57e-04	1.14e-04	1.45e-06
	epochs	4159	717	190

Table 6: The errors and epochs for SNNW-G on different hidden layer depth.

Hidden Layer	M	60	100	300
0	$\ e\ _{L^2}$	1.76e-04	9.40e-06	1.30e-06
	epochs	4026	2488	1894
1	$\ e\ _{L^2}$	2.61e-03	2.99e-04	2.10e-07
	epochs	2455	912	215
2	$\ e\ _{L^2}$	2.94e-02	2.59e-04	4.81e-05
	epochs	4550	1356	360
3	$\ e\ _{L^2}$	1.44e-04	3.64e-05	1.80e-06
	epochs	380	349	196
4	$\ e\ _{L^2}$	1.23e-04	1.92e-05	6.73e-06
	epochs	314	362	273
5	$\ e\ _{L^2}$	6.90e-04	5.98e-06	6.32e-06
	epochs	757	335	208
6	$\ e\ _{L^2}$	2.25e-04	2.00e-04	1.50e-05
	epochs	1717	553	307

Table 7: The errors for SNNW-R on different hidden layer depth.

Hidden Layer	M	60	100	300
0	$\ e\ _{L^2}$	8.40e-05	2.88e-05	3.83e-06
1	$\ e\ _{L^2}$	9.35e-04	8.91e-06	3.54e-07
2	$\ e\ _{L^2}$	3.71e-04	4.14e-05	4.30e-03
3	$\ e\ _{L^2}$	8.97e-05	9.09e-07	1.15e-05
4	$\ e\ _{L^2}$	1.00e-04	5.07e-06	5.65e-06
5	$\ e\ _{L^2}$	2.36e-04	2.94e-05	4.88e-06
6	$\ e\ _{L^2}$	2.91e-04	1.09e-05	5.16e-06

3.2. Poisson equation

Consider the following Poisson equation with the Dirichlet boundary condition,

$$-\Delta u(x, y) = f, (x, y) \in \Omega,$$

where $\Omega = (0, 1)^2$. The Dirichlet boundary condition is

$$u(x, y) = 0, (x, y) \in \partial\Omega.$$

Take the exact solution as follows:

$$u(x, y) = \sin(\pi x) \sin(\pi y).$$

For SNNW, a two-dimensional composite Gaussian quadrature formula is applied to segment each dimension into 16 sub-intervals and allocate 4 points to each. The point-wise errors of SNNW-P, SNNW-G and SNNW-R are illustrated in Figure 7. Table 8 presents the relative L^2 errors for various methods including SNNW-P, SNNW-G, SNNW-R, PINN, DGM and DRM. This example serves to demonstrate the adaptivity of our algorithms. Notably, after 50000 training epochs, the relative L^2 errors of PINN, DGM and DRM are $2.71\text{e-}04$, $1.81\text{e-}03$ and $2.48\text{e-}04$, respectively. However, SNNW-P, SNNW-G and SNNW-R achieve relative L^2 errors of $1.67\text{e-}07$, $5.79\text{e-}07$ and $1.65\text{e-}07$, respectively, with significantly fewer epochs, specifically 359, 359 and 2000.

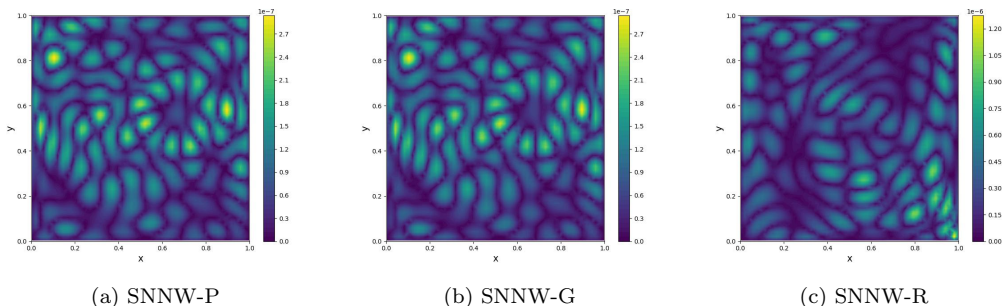


Figure 7: Point-wise errors of SNNW-P, SNNW-G and SNNW-R for Poisson equation.

Tables 9 and 10 present the performance of SNNW-P and SNNW-G across various numbers of sampling points and subspace dimension, maintaining a networks architecture of four hidden layers with 100 neurons each. SNNW-P

Table 8: The errors and epochs of different methods for the Poisson equation

Method	$\ e\ _{L^2}$	epochs
PINN	2.71e-04	50000
DGM	1.81e-03	50000
DRM	2.48e-04	50000
SNNW-P	1.67e-07	359
SNNW-G	1.65e-07	359
SNNW-R	5.79e-07	2000

and SNNW-G adopt the composite Gaussian quadrature, allocating 4 points per sub-interval in each direction and increasing sub-interval numbers for enhanced precision. Similar to the 1D Helmholtz equation, it becomes apparent that the error decreases with increasing both sampling points and subspace dimension. With a subspace dimension of 40, the error primarily ranges between 10^{-1} and 10^{-4} . Expanding the subspace dimension to 100, SNNW-P and SNNW-G can achieve the accuracy of 10^{-5} . With enough sampling points and further expansion of the subspace dimension, SNNW-P and SNNW-G can obtain and maintain the accuracy of 10^{-7} . Moreover, the training cost is low, and there only needs 300 to 2000 epochs.

The network setup and composite Gaussian quadrature rule of SNNW-R are identical with the ones of SNNW-P and SNNW-G. The numerical results of SNNW-R with fixed 2000 epochs are given in Table 11 for various numbers of sampling points and subspace dimension. With a subspace dimension of 100 and 150, the error is about 10^{-3} . Increasing the subspace dimension to 200, the error decreases promptly to 10^{-6} . As the number of sampling points and the subspace dimension further increase, SNNW-R achieves the accuracy of 10^{-7} .

Figure 7 illustrates the error variation with subspace dimension for 64×64 Gaussian integration points, and the error variation with respect to the number of integration points for a fixed subspace dimension of 300 for SNNW-P. Similarly, Figure 8 and 9 show the error variation with subspace dimension at a fixed number of 64×64 Gaussian integration points, and the error variation with the number of Gaussian integration points at a fixed subspace dimension of 300 for SNNW-G and SNNW-R, respectively. The number of training epochs for these experiments is ranging from 359 to 2000, and is

Table 9: The errors and epochs of SNNW-P across various numbers of sampling points and subspace dimension M for the Poisson equation

Points	M	40	60	80	100	200	300
12×12	$\ e\ _{L^2}$	2.26e-01	1.24e-01	1.22e-01	7.17e-02	6.66e-01	7.75e-01
	epochs	1482	936	669	572	398	320
16×16	$\ e\ _{L^2}$	7.18e-03	7.66e-03	1.38e-02	2.34e-03	7.30e-02	1.4e-01
	epochs	1536	972	701	612	427	340
20×20	$\ e\ _{L^2}$	1.71e-03	2.18e-03	6.25e-04	2.72e-04	1.05e-02	1.13e-02
	epochs	1452	1009	733	635	439	340
24×24	$\ e\ _{L^2}$	2.48e-04	2.42e-04	9.55e-05	8.20e-05	7.64e-04	8.00e-04
	epochs	1440	1029	743	649	445	354
32×32	$\ e\ _{L^2}$	1.97e-04	1.45e-04	6.80e-05	2.11e-05	4.48e-05	4.29e-05
	epochs	1388	1069	753	660	454	357
48×48	$\ e\ _{L^2}$	2.36e-04	1.27e-04	4.23e-05	1.48e-05	5.74e-07	3.89e-07
	epochs	1502	1076	768	674	459	361
64×64	$\ e\ _{L^2}$	3.07e-04	1.45e-04	7.56e-05	1.41e-05	2.06e-07	1.67e-07
	epochs	1392	1066	767	677	461	359

Table 10: The errors and epochs of SNNW-G across various numbers of sampling points and subspace dimension M for the Poisson equation

Points	M	40	60	80	100	200	300
12×12	$\ e\ _{L^2}$	4.16e-02	1.26e-01	2.91e-01	7.11e-02	6.86e-01	7.71e-01
	epochs	1846	947	668	571	398	320
16×16	$\ e\ _{L^2}$	5.39e-03	9.60e-04	1.00e-02	2.29e-03	7.22e-01	1.42e-01
	epochs	1527	988	716	612	427	340
20×20	$\ e\ _{L^2}$	3.31e-04	3.29e-04	6.32e-04	2.70e-04	1.02e-02	1.21e-02
	epochs	1380	1010	733	635	439	348
24×24	$\ e\ _{L^2}$	2.02e-04	3.17e-04	3.95e-04	8.31e-05	6.03e-04	7.99e-04
	epochs	1380	1035	741	650	445	354
32×32	$\ e\ _{L^2}$	2.52e-04	1.41e-04	6.64e-05	2.14e-05	4.60e-05	4.31e-05
	epochs	1487	1070	752	659	454	357
48×48	$\ e\ _{L^2}$	2.61e-04	1.12e-04	3.81e-05	1.53e-05	5.87e-07	3.83e-07
	epochs	1451	1065	770	675	459	361
64×64	$\ e\ _{L^2}$	2.42e-04	1.45e-04	6.26e-05	1.44e-05	2.07e-07	1.65e-07
	epochs	1426	1070	768	676	461	359

Table 11: The errors of SNNW-R with 2000 epochs across various numbers of sampling points and subspace dimension M for the Poisson equation

Points	M	100	150	200	250	300	500
20×20	$\ e\ _{L^2}$	1.42e-03	5.05e-03	2.24e-02	5.88e-01	5.53e-01	3.00e-01
24×24	$\ e\ _{L^2}$	1.42e-03	2.21e-03	1.60e-03	1.35e-04	1.73e-03	6.56e-03
32×32	$\ e\ _{L^2}$	1.97e-03	1.76e-03	1.15e-04	2.26e-04	1.06e-04	2.34e-04
48×48	$\ e\ _{L^2}$	1.91e-03	1.66e-03	3.23e-06	4.26e-06	3.23e-06	1.21e-05
64×64	$\ e\ _{L^2}$	1.65e-03	1.67e-03	2.12e-06	8.00e-07	5.79e-07	9.32e-07
72×72	$\ e\ _{L^2}$	2.05e-03	1.72e-03	2.10e-06	7.15e-07	5.18e-07	3.31e-07

significantly lower than that of PINN, DGM and DRM.

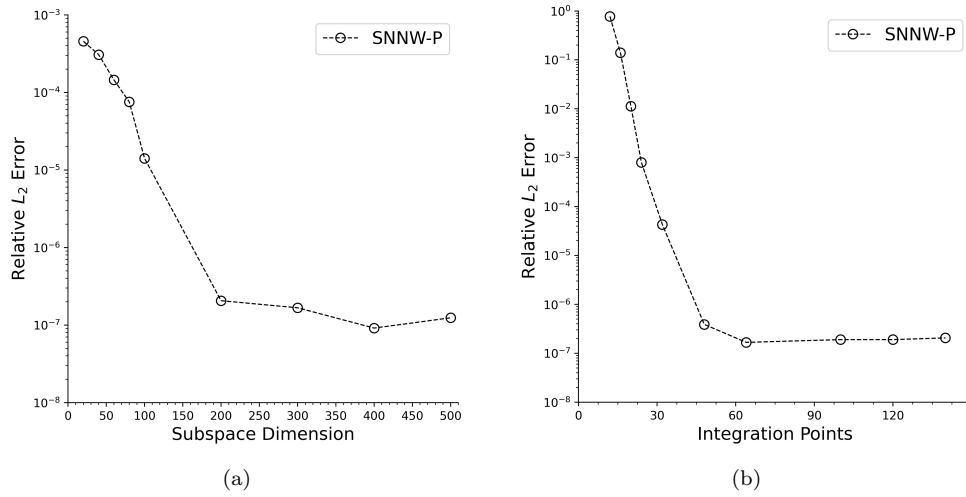


Figure 8: Error variation with subspace dimension at a fixed number of 64×64 integration points and error variation with the number of integration points at a fixed subspace dimension of 300 for SNNW-P.

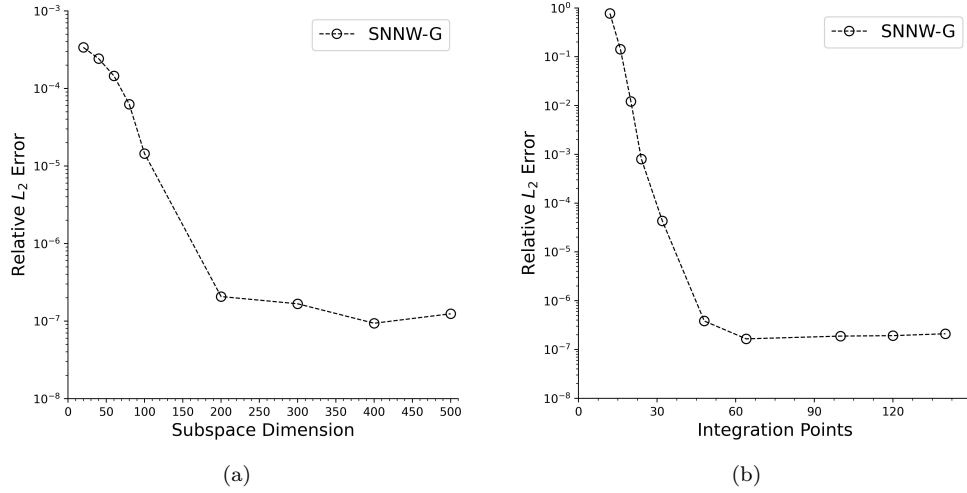


Figure 9: Error variation with subspace dimension at a fixed number of 64×64 integration points and error variation with the number of integration points at a fixed subspace dimension of 300 for SNNW-G.

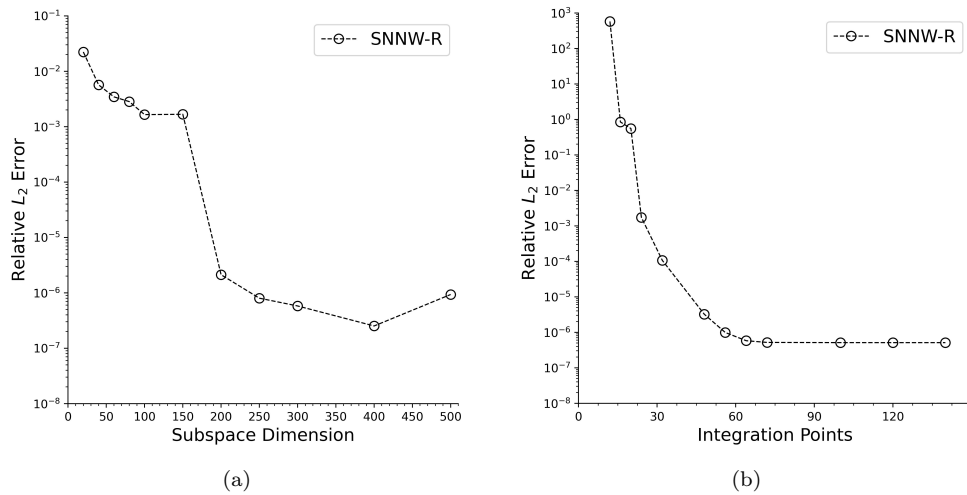


Figure 10: Error variation with subspace dimension at a fixed number of 64×64 integration points and error variation with the number of integration points at a fixed subspace dimension of 300 for SNNW-R.

3.3. Anisotropic diffusion equation

Consider the following diffusion equation with anisotropic diffusion coefficient on the domain $\Omega = (0, 1)^2$,

$$\begin{aligned} -\nabla \cdot (\kappa(x, y) \nabla u) &= f(x, y), & (x, y) \in \Omega, \\ u(x, y) &= g(x, y), & (x, y) \in \partial\Omega, \end{aligned}$$

where

$$\kappa(x, y) = \begin{pmatrix} k_1 & 0 \\ 0 & k_2 \end{pmatrix}.$$

We choose $f(x, y)$ and $g(x, y)$ such that the exact solution is $u(x, y) = \sin(\pi x) \sin(\pi y)$.

A two-dimensional composite Gaussian quadrature formula is utilized to divide each dimension into 16 sub-intervals, with 4 points per sub-interval. This strategy leads to 4096 sampling points. Table 12 and 13 illustrate the relative L^2 errors of different methods for solving the anisotropic diffusion equation with various anisotropic ratios. PINN, DGM and DRM can persevere certain accuracy when the anisotropy is weak, and lose the accuracy when the anisotropy is very strong. However, even when the anisotropic ratio reaches $1 : 10^6$, SNNW-P attains the accuracy of $2.02\text{e-}06$, SNNW-G attains the accuracy of $2.07\text{e-}06$ and SNNW-R attains the accuracy of $1.56\text{e-}05$. This indicates that SNNW-P, SNNW-G and SNNW-R still can obtain high accuracy for the diffusion equation with strong anisotropic ratios. Compared to 50000 epochs of PINN, DGM and DRM, SNNW-P and SNNW-G only need several hundred of epochs. These tests further demonstrate that our method can achieves better accuracy with low training cost.

Table 12: The errors and epochs of PINN, DGM and DRM for the anisotropic diffusion equation with different anisotropic ratios.

Method	$k_1 : k_2$	$\ e\ _{L^2}$	epochs
PINN	$1 : 10^0$	9.54e-03	50000
	$1 : 10^1$	3.14e-02	50000
	$1 : 10^2$	1.68e-01	50000
	$1 : 10^3$	1.68e00	50000
	$1 : 10^4$	1.03e01	50000
	$1 : 10^5$	9.62e01	50000
	$1 : 10^6$	1.04e01	50000
DGM	$1 : 10^0$	1.81e-03	50000
	$1 : 10^1$	2.67e-02	50000
	$1 : 10^2$	7.55e-01	50000
	$1 : 10^3$	1.91e00	50000
	$1 : 10^4$	1.00e01	50000
	$1 : 10^5$	1.02e01	50000
	$1 : 10^6$	1.02e01	50000
DRM	$1 : 10^0$	2.48e-04	50000
	$1 : 10^1$	1.44e-04	50000
	$1 : 10^2$	1.37e-04	50000
	$1 : 10^3$	2.16e-01	50000
	$1 : 10^4$	4.77e-02	50000
	$1 : 10^5$	4.97e-04	50000
	$1 : 10^6$	2.06e-02	50000

Table 13: The errors and epochs of SNNW-P,SNNW-G and SNNW-R for the anisotropic diffusion equation with different anisotropy ratios.

Method	$k_1 : k_2$	$\ e\ _{L^2}$	epochs
SNNW-P	$1 : 10^0$	1.67e-07	359
	$1 : 10^1$	7.37e-07	442
	$1 : 10^2$	9.94e-07	723
	$1 : 10^3$	1.94e-06	809
	$1 : 10^4$	2.04e-06	773
	$1 : 10^5$	2.11e-06	766
	$1 : 10^6$	2.02e-06	765
SNNW-G	$1 : 10^0$	1.65e-07	359
	$1 : 10^1$	7.14e-07	442
	$1 : 10^2$	1.03e-06	723
	$1 : 10^3$	2.05e-06	809
	$1 : 10^4$	2.07e-06	773
	$1 : 10^5$	2.11e-06	766
	$1 : 10^6$	2.07e-06	765
SNNW-R	$1 : 10^0$	5.79e-07	2000
	$1 : 10^1$	1.96e-06	2000
	$1 : 10^2$	6.96e-06	2000
	$1 : 10^3$	1.28e-05	2000
	$1 : 10^4$	1.42e-05	2000
	$1 : 10^5$	1.52e-05	2000
	$1 : 10^6$	1.56e-05	2000

4. Conclusion

In this paper, we present SNNW for solving the partial differential equation in weak form with high accuracy. The basic idea of SNNW is to use some functions based on neural networks as base functions to span a subspace, then find an approximate solution in this subspace. Training base functions and finding an approximate solution can be separated, that is different methods can be used to train these base functions, and different methods can also be used to find an approximate solution. We train these base functions by minimizing the loss function, which can be based on different form, such as the strong form and the weak form. In this paper, we use PINN, DGM or DRM to train these base functions in the subspace, and use the Galerkin method to solve the partial differential equation. Our method can achieve high accuracy with low cost of training. Numerical examples show that the cost of training these base functions is low, and only several hundred to two thousand epochs are needed for most tests. The error of our method can fall below the level of 10^{-7} for some tests.

Acknowledgements

This work is partially supported by National Natural Science Foundation of China (12071045) and Funding of National Key Laboratory of Computational Physics.

References

- [1] J. Chen, X. Chi, W. E and Z. Yang, Bridging traditional and machine learning-based algorithms for solving PDEs: the random feature method, *J. Mach. Learn.* 1 (2022)268-298.
- [2] X. Chi, J. Chen, Z. Yang, The random feature method for solving interface problems, *Comput. Methods Appl. Mech. Eng.*, 420(2024)116719.
- [3] S. Dong, Z. Li, Local extreme learning machines and domain decomposition for solving linear and nonlinear partial differential equations, *Comput. Methods Appl. Mech. Engrg.* 387 (2021) 114129.
- [4] W. E, B. Yu, The deep Ritz method: a deep learning-based numerical algorithm for solving variational problems, *Commun. Math. Stat.*, , 6(2018)1-12.

- [5] A. Jagtap, E. Kharazmi, G. Karniadakis, Conservative physics-informed neural networks on discrete domains for conservation laws: applications to forward and inverse problems, *Comput. Methods Appl. Mech. Eng.*, 365(2020)113028.
- [6] A. Jagtap, Z. Mao, N. Adams, G. Karniadakis, Physics-informed neural networks for inverse problems in supersonic flows, *J. Comput. Phys.*, 466(2022)111402.
- [7] Y. Li, F. Wang, Local randomized neural networks methods for interface problems, *arXiv:2308.03087*,2023.
- [8] Y. Liao, P. Ming, Deep Nitsche method: deep Ritz method with essential boundary conditions, *Commun. Comput. Phys.*, 29(2021)1365-1384.
- [9] L. Liu, S. Liu, H. Xie, F. Xiong, T. Yu, M. Xiao, L. Liu, H. Yong, Discontinuity computing using physics-informed neural networks, *J. Sci. Comput.*, (2024) 98:22.
- [10] L. Lyu, Z. Zhang, M. Chen, J. Chen, MIM: A deep mixed residual method for solving high-order partial differential equations, *J. Comput. Phy.*, 452(2022)110930.
- [11] A. Paszke, S. Gross, F. Massa, A. Lerer, J. Bradbury, G. Chanan, T. Killeen, Z. Lin, N. Gimelshein, L. Antiga, et al., Pytorch: An imperative style, high-performance deep learning library, *Advances in neural information processing systems*, 32 (2019)8026-8037.
- [12] R. Patel, I. Manickam, N. Trask, M. Wood, M. Lee, I. Tomas, E. Cyr, Thermodynamically consistent physics-informed neural networks for hyperbolic systems, *J. Comput. Phys.*, 449(2022)110754.
- [13] M. Raissi, P. Perdikaris, G. Karniadakis, Physics-informed neural networks: A deep learning framework for solving forward and inverse problems involving nonlinear partial differential equations, *J. Comput. Phys.*, 378(2019) 686-707.
- [14] Y. Shang, F. Wang and J. Sun, Randomized neural network with Petrov-Galerkin methods for solving linear and nonlinear partial differential equations, *Communications in Nonlinear Science and Numerical Simulation*,127(2023) 107518.

- [15] H. Sheng, C. Yang, PFNN: A penalty-free neural network method for solving a class of second-order boundary-value problems on complex geometries, *J. Comput. Phys.*, 428(2021)110085.
- [16] J. Sirignano, K. Spiliopoulos, DGM: A deep learning algorithm for solving partial differential equations, *J. Comput. Phys.*, 375(2018)1339-1364.
- [17] J. Sun, S. Dong and F. Wang, Local randomized neural networks with discontinuous Galerkin methods for partial differential equations, *J. Comput. Appl. Math.*, 445(2024)115830.
- [18] Y. Wang, Tensor neural network and its application for solving partial differential equations, Academy of Mathematics and Systems Science, Chinese Academy of Sciences, Doctoral Dissertation(in Chinese), 2023.
- [19] Y. Wang, P. Jin, H. Xie, Tensor neural network and its numerical integration, arXiv:2207.02754,2023.
- [20] Y. Wang, Z. Lin, Y. Liao, H. Liu, H. Xie, Solving high dimensional partial differential equations using tensor neural network and a posteriori error estimators, arXiv:2311.02732,2023.
- [21] Z. Xu, Z. Sheng, Subspace method based on neural networks for solving the partial differential equation, arXiv:2404.08223,2024.
- [22] Y. Yao, J. Guo, T. Gu, A deep learning method for multi-material diffusion problems based on physics-informed neural networks, *Comput. Methods Appl. Mech. Engrg.* 417 (2023) 116395.
- [23] J. Ying, J. Liu, J. Chen, S. Cao, M. Hou, and Y. Chen, Multi-scale fusion network: A new deep learning structure for elliptic interface problems, *Appl. Math. Modelling*, 114(2023) 252-269.
- [24] Y. Zang, G. Bao, X. Ye, H. Zhou, Weak adversarial networks for high-dimensional partial differential equations, *J. Comput. Phys.*, 411(2020)109409.